6 Coalescence of bubbles in surfactant solutions

We can never, in principle, observe things, only the interaction between things.
Paul Davies, The Textual Society, E.Taborsky, University of Toronto Press, Buffalo, Canada, 1997.

6.1 The formation, break-up and coalescence of bubbles in surfactant solutions

Vigorous stirring or agitation of a weak surfactant solution in a vessel (such as a stirred tank) causes entrapment of air in the liquid and produces bubbles, resulting in an increase in gas fraction and a decrease in bubble size. During this continuous process, impaction, disruption, disintegration and coalescence of bubbles also occur within the bubble swarm. The disintegration pressure, which acts to break apart large bubbles into smaller ones, tends to originate from the high kinetic energy and the additional stresses from turbulence in the bulk liquid. Although the bubbles become deformed, the capillary pressure which originates from the curvature and surface tension gradients tends to restore the bubble shape. In fact, the overall process may be considered as an equilibrium between these opposing forces, although other processes such as deformation (compaction) of bubbles may occur as they swirl in the bulk solution. Other types of interactions caused by, for example, shear, gravitational and buoyancy forces are also important, but provided some of the bubbles have sufficient elasticity to survive, they will eventually rise to the surface and assemble to produce the foam head.

In the gas/liquid dispersions, where the kinetic energy of the fluid phase is high, the dimensionless Weber number (W_e) can be used to define the break-up process in terms of the ratio between disrupting inertial shear stress and interfacial stress, which acts as stabilizing forces (the Laplace pressure). This has been expressed according to Nguyen and Schulze (1) by the equation

$$W_e(1) = \text{Splitting pressure}/\text{Capillary pressure} = \rho_\ell V_{brv}^2 \, r_b/\gamma \qquad (6.1)$$

where W_e (1) signifies the Weber number for a single bubble, ρ_ℓ is the density of the liquid, r_b is the radius of the bubble, γ is the surface tension and V_{brv} is the bubble rise velocity. For two bubbles 1 and 2 approaching collision, the Weber number is expressed according to Duineveld (2) by the equation

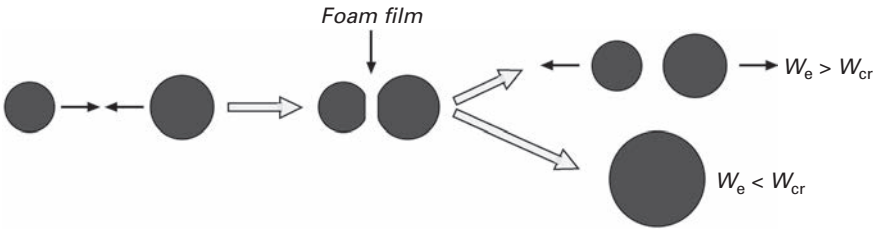

Fig. 6.1 Basic steps in the collision between two bubbles under high kinetic energy which may lead to coalescence or re-stabilization. From ref (3).

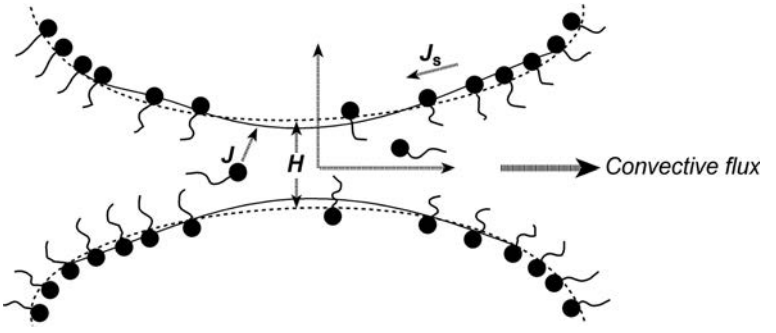

Fig. 6.2 Approaching bubbles under low kinetic energy causes stretching and redistribution of surfactant which may eventually lead to coalescence. The flow of surfactant along the interface (*Js*) and the diffusion and adsorption of surfactant from the bulk to the interface (*J*) act to compensate the stretching process.

$$W_e(1,2) = (\rho_\ell V_{av}^2/2\gamma)(1/r_{b1} + 1/r_{b2}) \tag{6.2}$$

where the two bubbles approaching contact have radii of r_{b1} and r_{b2} and V_{av} is the bubble approach velocity. If W_e exceeds a critical value (W_{cr}) the bubbles bounce after colliding, and if W_e is less than W_{cr}, they coalesce. These two different situations are illustrated in Fig. 6.1. The presence of adsorbed surfactant plays a role in inhibiting the bubble coalescence, which reduces the value of the critical Weber number.

However, in systems where the kinetic energy of the fluid is relatively low (e.g. in bubble columns where gas is released from the base of a column and relatively low gas velocities are involved), an alternative situation exists. In this case, since the breakage of bubbles may be negligible, the quantity of dispersed gas bubbles will depend mainly on coalescence. Although this process can occur within milliseconds, hydrodynamic flow of liquid outward from the film and close-range interfacial forces play an important role when the curved interfaces are in close proximity. Deformation and curvature changes occur and the film separating the bubbles may become stretched as shown, but the flow of a chemical surfactant along the interface and the diffusion and adsorption of surfactant from bulk solution act to stabilize the film, as shown in Fig. 6.2.

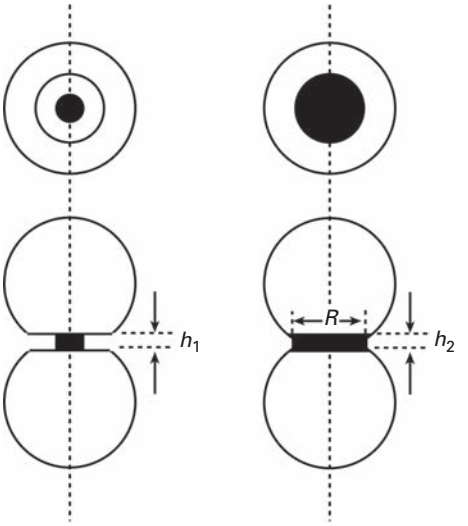

Fig. 6.3 Stretching of the film between two coalescing bubbles in which the thickness decreases from h_1 to h_2. The dimensions of the film are exaggerated. From ref (4).

It is difficult to calculate the exact shape of the bubble interface, and numerical solutions are needed since the geometry, hydrodynamics and intermolecular interactions are all interlinked. In fact, inverse curvature (dimpling) can sometimes occur at close contact. An outward flow of liquid from the region of closest approach occurs, causing a redistribution of surfactant at both the interface and within the thin film region. Surface gradients may also cause the inward flow of liquid and the diffusion and re-adsorption of surfactant from solution. This can lead to relaxations and viscoelastic effects which act to resist deformation. Following the coalescence between two bubbles, the resultant bubble oscillates until the excess energy is released from the system. The fluid viscosity acts as a damper to such oscillations, and both the surface energy and area of the bubble surface decrease.

6.2 The role of surface tension gradients in coalescence

In aqueous solutions containing fairly high concentrations of certain types of inorganic electrolytes that are well known to act as weak surfactants, the degree of bubble coalescence in columns may be reduced. In 1969, Marrucci (4) proposed a theory based on the assumption that the flow, during the initial drainage of the liquid film between two bubbles, proceeds radially outward from the central axis of the curved interface. For mobile interfaces, the flow velocity is uniform through the film (plug flow). This it leads to the expansion of a small circular surface area from the central axis, causing stretching of the film (similar to a sheet of rubber) causing a decrease in thickness (from h_1 to h_2), as shown in Fig. 6.3.

During this process, as the surface area of the thin film element increases, the solute concentration within the film is also increased in relationship to that on the remainder of the film surface. The higher salt concentration produces an increase in surface tension in the film, and this causes a force to develop which acts in the opposite direction to the flow at the gas/liquid interface boundary. This force acts as a resistance to the thinning, and provided the solute concentration is sufficiently high, the interface becomes to some extent immobilized; this situation was considered as a critical quasi-equilibrium. In the Marrucci model (4), the transport of solute to relieve the gradient in surface tension was taken into consideration and an expression was developed for the concentration of solute necessary to immobilize the interface in coalescing bubbles. The expression is based on the change in surface excess of solute which accompanies the expansion of the liquid film during coalescence. Based on this model Prince and Blanch (5) in 1990 defined an equibrium solute (electrolyte) concentration by C_t or the "critical transition concentration," is related to various other parameters in the system and is expressed by the equation

$$C_t = 0.084\, n_i\, R_g T\, \left(A_H^2 \gamma / r_b\right)^{1/3} / (d\gamma/dc)^2 \tag{6.3}$$

where R_g is the gas constant, A_H is the Hamaker constant, r_b is the radius of the bubble, $d\gamma/dc$ is the surface tension gradient and n_i is the number of ions produced on dissociation of the solute. This equation stresses the importance of the square of the surface tension gradient $(d\gamma/dc)^2$ which is related to the surface elasticity and acts to delay or prevent the coalescence process. In fact, the value of C_t can be regarded as a stability/instability criterion.

In 1971, coalescence experiments were carried out in varying concentrations of electrolyte by Lessard and Zieminsky (6). Two identical bubbles were formed at adjacent capillary tubes, and from this study, both a transition concentration (where 50% of the bubbles coalesced and 50% remained stable) and a maximum stability concentration (where 100% of the bubbles failed to coalesce) were quantified. In these experiments, the Marrucci model was found to satisfactorily account for the results in inorganic electrolytes but was found unsuitable to explain coalescence in the presence of weak organic surfactants. In 1990, Prince and Blanch (5) carried out a series of experiments in both water and salt solution to study the coalescence and break-up of air bubbles in a sparged bubble column. The system was modeled by considering collision due to turbulence, buoyancy and laminar shear. Bubble break-up was analyzed in terms of bubble interactions and turbulent eddies. A reasonable agreement between the experimental data and the model was obtained. Prince and Blanch (5) also amended the Marrucci model and included a more detailed analysis of film drainage and also of the influence of both inertia and a retarded van der Waals forces within the film drainage regime. The alternative expression for the transition electrolyte concentrations for bubble coalescence was derived and expressed as

$$C_{PB} = 1.18\, n_i [(A_R \gamma / r_b)^{1/2} R_g T] / (d\gamma/dc)^2 \tag{6.4}$$

where, n_i is the number of ions produced on dissociation of the solute and A_R is the retarded Hamaker constant. Further extensions to the "Marrucci theory" were developed. Most of these models define a proportionality between the transition concentration and the parameter $(d\gamma/dc)^2$ which describes the change in surface tension with concentration and this which became known as the "Marangoni factor." Several other similar theories have been developed, and allowances have been made to include different types of ionic species which give different values of $d\gamma/dc$.

6.3 Relationship between elasticity and critical transition concentration C_t

According to the definition of Gibbs, the elasticity of a thin liquid film stabilised by surfactant can be expressed by

$$E = \frac{d\gamma}{dlnA} = A\left(\frac{d\gamma}{dA}\right) = A\left(\frac{d\gamma}{dc}\right)\left(\frac{dc}{dA}\right) \tag{6.5}$$

where A is the area of the film, or $2A$ in the case of a film with two interfaces. If we define the thickness of the film as h and volume as V, then $V = Ah$, and on rapid stretching of the film, a small change in concentration results, which can be expressed by

$$dc = -\frac{2\Gamma A}{Ah} \tag{6.6}$$

where Γ is the surface excess of the surfactant. On substituting the Gibbs adsorption equation, the elasticity of the two interfaces can be expressed as

$$E = 4c\frac{\left(\frac{d\gamma}{dc}\right)^2}{k_B Th} \tag{6.7}$$

where k_B is the Boltzman constant and T is the temperature.

Changes in film thickness cause changes in the elastic response, which tends to prevent rupture of the film by resisting coalescence. Surface elasticity in solutions of weak electrolytes is usually considered to result from a decrease in surface tension associated with an expansion of the interface, which leads to a reduction in the amount of adsorbed material. However, in this equation $d\gamma/dc$ can be positive or negative, and hence it can also be applied to an increase in surface tension caused by a depletion of ions which occurs for many inorganic electrolytes. Christenson and Yaminsky (7) carried out a series of experiments in bubble columns showing that $(d\gamma/dc)^{-2}$ could be related to the critical transition concentration by using experimental coalescence data obtained from several inorganic electrolytes as reported by Craig and coworkers (8).

6.4 Experimental studies on bubble coalescence

Bubble coalescence has been traditionally studied by the chemical engineering community by gently agitating liquids in large columns and tanks or in sparging columns. However, bubbles are rarely monodisperse and the effects caused by dissolved gas gradients and drainage cannot be easily neglected. Although only statistical data on changes in bubble population can be obtained from these studies, some insight into the coalescence process is possible. In these experiments, the contact and coalescence time can be determined from changes in bubble size distribution and changes in the population of bubble clouds under specific flow conditions. Since these experiments are usually difficult to perform, many coalescence studies have been carried out using more simplified model systems. For example, 2D bubble rafts have been constructed from monolayers of bubbles, and also experiments with ascending single bubbles or freely rising bubble pairs designed to rise side by side have been carried out. Coalescence experiments have also been performed on bubble pairs, suspended at the ends of capillaries, and the pressure balance technique has been used to study the coalescence of an isolated thin liquid film. Some of these techniques are discussed in some detail in the following sections.

6.4.1 Bubble swarm and single bubbles

Many coalescence experiments have been carried out on bubble swarms which were weakly stabilized with low concentrations of short-chain alcohols or inorganic electrolytes. Kirkpatrick and Locket (9) used high-speed photographs to record changes in bubble clouds in aqueous salt solutions, but the results revealed the complete absence of coalescence, which was attributed to the high approach velocities of the bubbles. Further experiments with single, rising bubbles that reach the air/liquid interface in pure liquids revealed the occurrence of two different types of coalescence processes: (a) rapid coalescence at low approach velocity and (b) delayed coalescence at high approach speed, in which bubbles made initial contact for a few milliseconds before coalescence, and in some cases the bubbles bounced back from the interface.

6.4.2 2D Bubble rafts

Several coalescence experiments have been carried out using bubble rafts. Burnett and coworkers (10) prepared layers of 2D-dispersed bubbles confined between two glass plates. In order to avoid disproportionation monodispersed bubbles were used and coalescence was achieved by warming up the foam cell. A critical breakdown or disintegration of the thin film structure was observed which involved a rapid cascade mechanism, and the critical break-time was found to be dependent on the initial conditions and the rate of increase in temperature. Cascade breakdown processes have also been frequently observed in 3D foam systems. Ritacco and coworkers (11) prepared hexagonally packed 2D bubble rafts on the surface of a liquid subsurface.

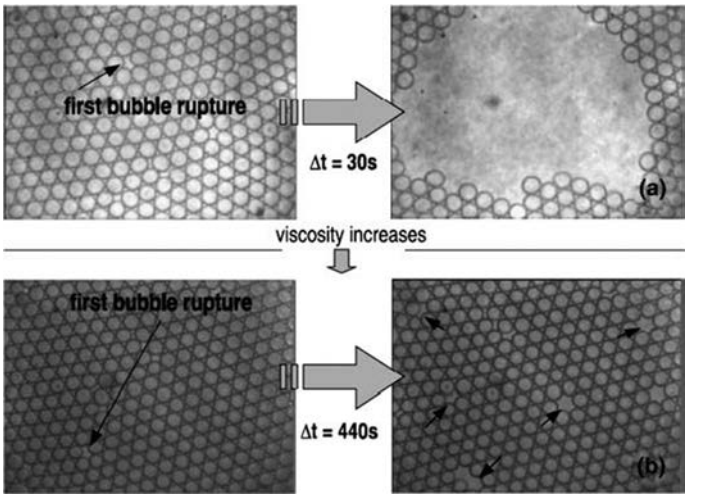

Fig. 6.4 Monodispersed bubble raft with low bulk viscosity (top) in which fast coalescence occurs through catastrophic events; with a bubble raft stabilized by the same surfactant and with much higher bulk viscosity, coalescence slowed through isolated events (as indicated at the bottom). From ref (11).

The interfacial viscoelastic properties were varied by using different surfactants, but it was found that the bulk viscosity of the foaming solution had a dominant role on the dynamics of film rupture. Low bulk viscosities caused cascade film rupture, whereas in high viscosity systems, coalescence occurred through isolated events, as illustrated in Fig. 6.4.

6.4.3 Coalescence at the moment of bubble creation

Kracht and Finch (12) studied the coalescence of bubbles at the moment of bubble creation using an acoustic technique. Bubbles were generated from a capillary orifice which was constructed into the base of an acrylic tank containing a weak foaming surfactant solution. From the sound trace characteristics (a decaying sinusoidal event) it was possible to distinguish between a coalescence and a non-coalescence event. The acoustic emissions recorded with a hydrophone were relayed to an amplifier and a computer. By careful control of the experimental conditions, such as a constant gas flow rate and temperature, it was possible to link the acoustic signal generated for a given bubble frequency to the bubble formation and coalescence event. By increasing the gas flow rate (at a fixed concentration of surfactant) to a critical value, it was possible to induce coalescence, and this value of the critical gas flow rate corresponding to the onset of coalescence was recorded. In Fig. 6.5(a), the experimental set-up is shown, and in Fig. 6.5(b), the frequency analysis, which records the generation event for bubbles of different sizes, is presented.

A characteristic image recording of the sequence of steps is shown in Fig. 6.6 for the generation and coalescence event in a solution containing a commercial frother

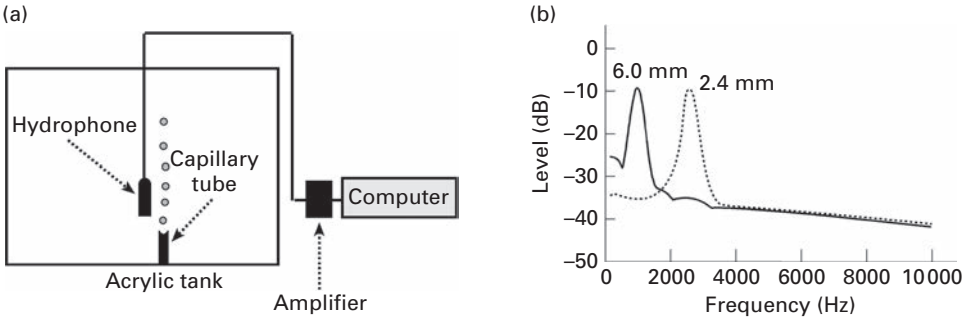

Fig. 6.5 (a) Experimental set-up for measuring the acoustic emission of bubbles and coalescence at a capillary tube and (b) frequency analysis of sound produced by generation of two bubbles of 2.4 and 6 mm. From ref (12).

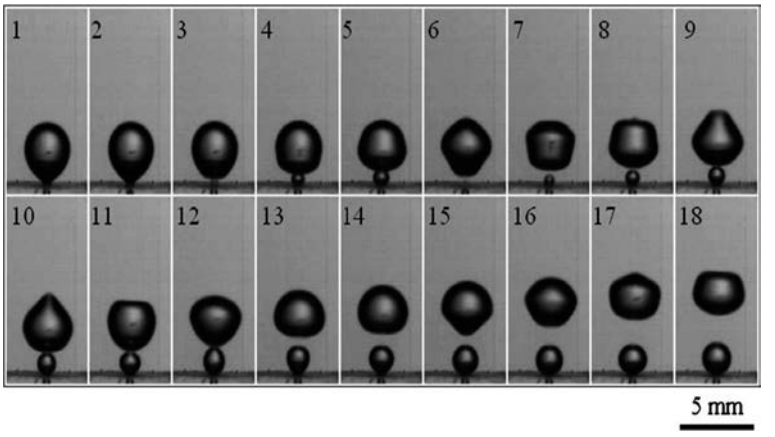

Fig. 6.6 Typical sequence of images (1 ms apart) of bubble formation with coalescence with two subsequent bubbles (frames 5 and 8). Dowfroth 250 (conc = 0.04 mmol/L). From ref (12).

Dowfroth 250; $CH_3(PO)_3OH$, where P is propylene oxide. The bubble detaches from the capillary (Fig. 6.6. frame 3) and the subsequent bubble (Fig. 6.6. frame 4) contacts the first bubble and coalesces with it (Fig. 6.6. frame 6). From the sound trace which corresponds to the image sequence, the transition point (quantified by the magnitude of the gas flow rate) that corresponded to the change from the non-coalescence to the coalescence state was determined as a function of surfactant concentration.

Using this technique, experiments were carried out with a series of low molecular weight, short-chain *n*-alcohols, and the results were compared to three commercial flotation nonionic frothers. These chemicals are used at low concentration in traditional industrial flotation practices to weakly stabilize bubbles which float hydrophobic minerals such as graphite and coal. From the results shown in Fig. 6.7, which relate the critical gas flow rate to the concentration, the effectiveness of the surfactant to retard coalescence

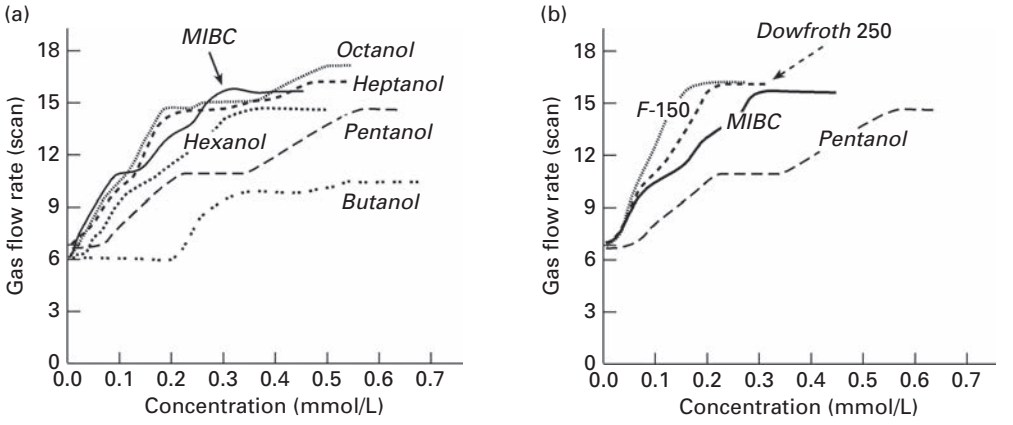

Fig. 6.7 Plots of gas flow rate corresponding to coalescence for (a) *n*-alcohols (MIBC included), (b) commercial nonionic frothers compared to pentanol. From ref (12).

increases with increasing chain length (decrease in surface activity) for the series of *n*-alcohols and also increases with concentration. However, the relationship appears to be only quantitative, since the results for the heptanol C_7 are about the same as for the octanol C_8.

The results for this homogeneous series of short-chain alcohols were explained by a total elastic stress model. In this model, the interfacial rheology of the bubbles was expressed by both elastic and viscous components, which acted to resist the stretching and deformation of the film. It was argued that the increase in elasticity was counterbalanced by the reduction in diffusion/adsorption rate of the soluble alcohol from the adjacent liquid. In addition to these frother systems, experiments were carried out in NaCl solution using the acoustic emission technique, but a less well-defined transition point between coalescence and non-coalescence events was recorded.

6.4.4 Freely rising single bubble using a laser detector

Jameson and Parekh (13) reported coalescence experiments in which bubbles were released from an orifice and allowed to rise to the surface of an aqueous solution. The equipment used for the experiments is shown in Fig. 6.8.

A laser beam was placed just below the surface of the liquid with a detector in the light path so that any disturbance at the surface by the bubble could be recorded by a break in the beam, and the arrival of the bubble at the surface was monitored from an oscilloscope trace. The time of persistence (the time of drainage of the liquid film trapped between bubbles) was determined from the time difference between arrival and bursting of a bubble and recorded as a function of solute concentration. In this study, a similar series of short-chain alcohols as used by Kracht and Finch (12) were compared, and it was found that the persistence time increased with increase in concentration for all the

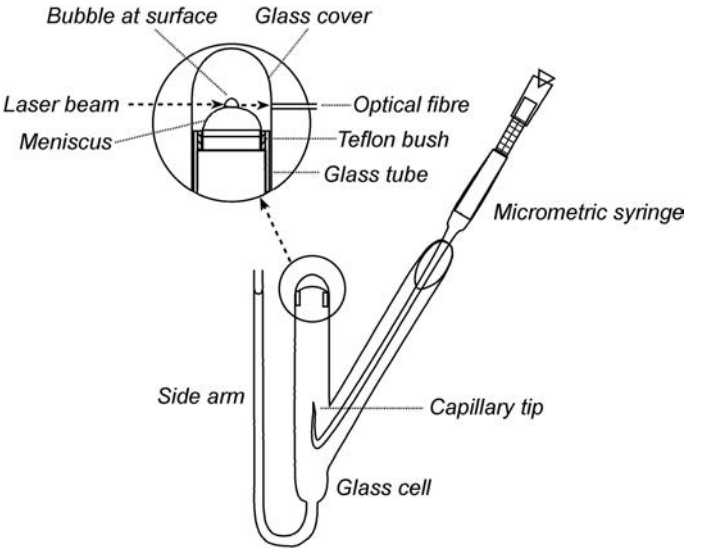

Fig. 6.8 Schematic diagram of the apparatus used for observing the persistence time of bubbles at the air/solution interface. From ref (13).

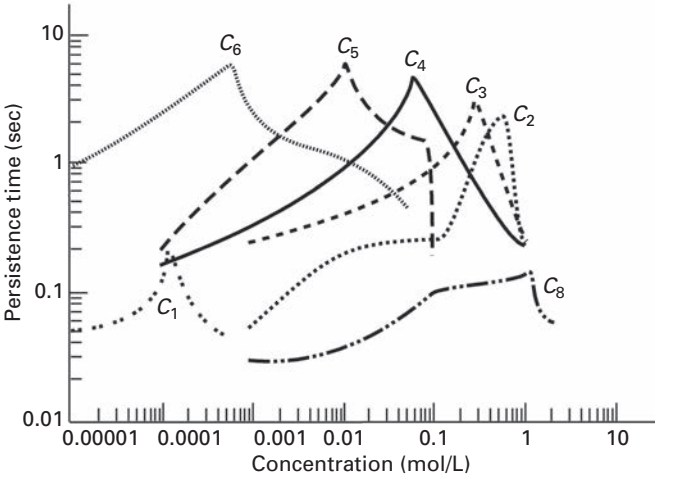

Fig. 6.9 Persistence times for *n*-alcohols: bubble diameter versus concentration. From ref (13).

alcohols until a maximum value was reached, but then it began to decrease as shown in Fig. 6.9.

These results support the very early work by Bartsch in 1920 (14), in which simple foam-shaking tests were conducted using a series of short-chain alcohols and acids where a maximum in the foam persistence time was found to occur and which corresponded to an optimum surfactant concentration. In further experiments, Jameson and

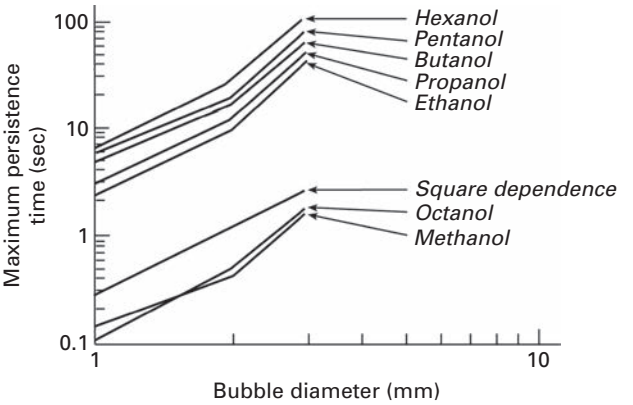

Fig. 6.10 The maximum persistence time versus bubble size for bubbles stabilized by a series of short-chain low molecular weight alcohols. A line is shown, for comparison purposes, which indicates a square-law dependency. From ref (13).

Parekh (13) determined the influence of bubble size on the maximum bubble persistence time, and it was found that the maximum persistence time increased with increase in bubble diameter for all the short-chain alcohols, as indicated in Fig. 6.10.

From the data, the bubble persistence time (t_p) could be expressed by the empirical equation

$$t_p = K_p h_b^n \tag{6.8}$$

where h_b is the bubble size and K_p was a constant. It was suggested that the exponent n was a function of bubble size, and other parameters in the equation were probably related to dimensionless fluid dynamic number groups such as Reynolds (R_e) and Weber (W_e) numbers. The values of K_p varied from solute to solute and probably included parameters associated with the fluid and interfacial properties, including intermolecular forces and electrostatic effects. The alcohol concentration which corresponded to maximum persistence time was termed "maximum stability concentration" (C_{max}), and a direct correlation was established between C_{max} and the number of carbons in the chain length, as shown in Fig. 6.11.

These results were discussed in terms of the surface activity of the solute using a similar approach to Kracht and Finch (12). Although the surface activity of the solute increased with the increase in both concentration and chain length of the alcohol (at the same concentration), there did not appear to be a simple correlation between the maximum t_p and γ or the surface excess per molecule at the interface. However, it was found that the concentration of maximum persistence (C_{max}) could be correlated with the function $\gamma^{1/2} (d\gamma/dc)^2$. This relationship was reported in the earlier coalescence studies by Prince and Blanch (6b), and it confirmed the importance of the surface tension gradients in bubble coalescence.

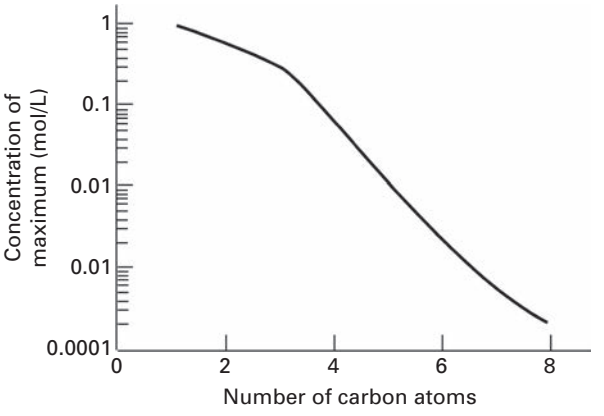

Fig. 6.11 Maximum stability concentration C_{max} versus carbon number for low molecular weight short chain *n*-alcohols. From ref (13).

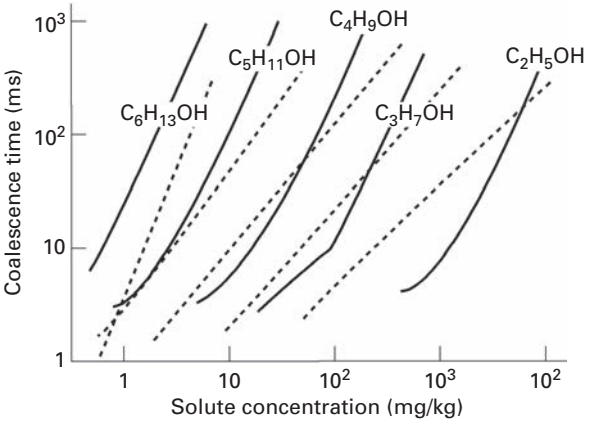

Fig. 6.12 Double logarithmic plots of both experimental and calculated times versus solute concentration for five alcohols: solid line – experiment; dashed line – based on modified Marrucci theory. From ref (15).

6.4.5 Growing bubbles from adjacent nozzles

Sagert and coworkers (15) grew equal-sized bubbles from adjacent nozzles in aqueous solution and demonstrated the influence of small amounts of alcohol on the coalescence times compared to the coalescence times of bubbles in pure water (determined using high-speed photography). Experiments were carried out with a homogeneous series of *n*-alcohols (C_2–C_6), and the results are shown in Fig. 6.12.

From this study, it was reported that for concentrations of amyl alcohol as low as 10^{-8} M, the coalescence time was reduced. It was also found that the coalescence time was either proportional to the alcohol concentration (for ethanol and propanol) or

approximately to a second-power relationship of alcohol concentration (in the cases of *n*-pentyl and *n*-hexyl alcohol). A non-equilibrium model was developed and it was also based on the early Marrucci theory (4), which considered surfactant diffusing to the film during the thinning and rupture processes. An equation was derived which enabled the total time for the coalescence process to be estimated from the stretching time (t_s) and breaking time (t_b). In order to calculate the stretching time, the criterion for mechanical stability of a thin film segment was used.

From this approach, values of t_s and t_b as a function of film thickness were calculated separately. However, it was found necessary to also take into account the short-time inertia effects to formulate an inertial time (t_{in}) for the movement of the liquid film. In addition, the rupture time, which was derived from the model of Sharma and Ruckenstein (16) for the lifetime of a liquid film of constant thickness, was included. In this model, surface perturbations of variable wavelength were considered and an equation derived which defined the breaking time as a function of wavelength using hydrodynamic linear stability theory. Final estimates of coalescence time were calculated from values of t_s (the stretching time), and values of t_b (the breaking time) were estimated from plots of $t_s + t_b$ versus the film thickness. This theoretical approach enabled plots of the coalescence time versus solute concentration to be made and the data are shown as dashed lines in Fig. 6.12. The results are shown to be in general agreement with the experimental results in predicting the order of performance. The magnitude for the film breaking times was also found to be in reasonable agreement with experimental coalescence times.

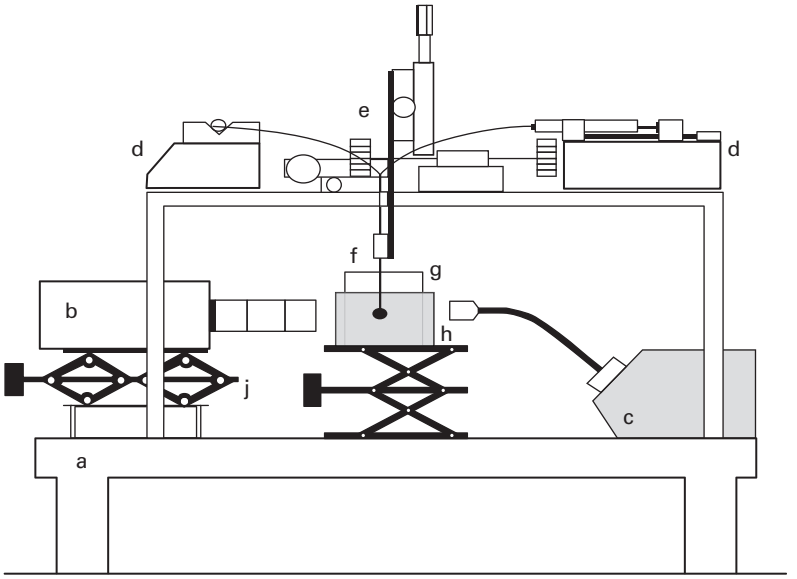

Fig. 6.13 Experimental set-up (a) vibration-free table, (b) CCD camera, (c) light source, (d) microsyringe and pump, (e) stage positioners, (f) stainless steel capillary, (g) glass vessel, (h) perspex container, (j) lab jack support. From ref (17).

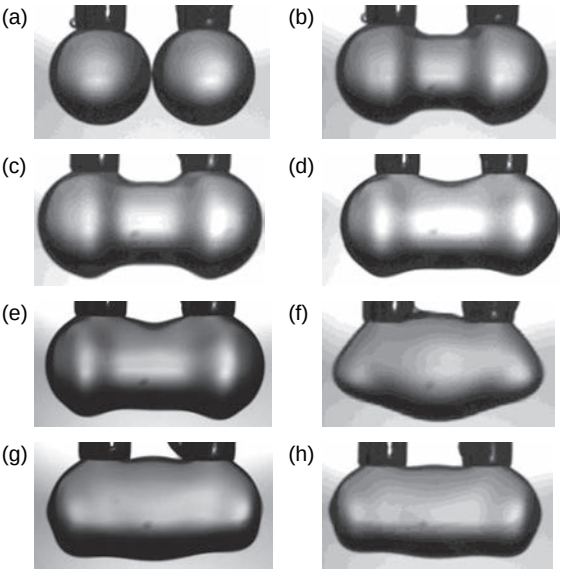

Fig. 6.14 Images of the oscillation behavior (a to h) following the coalescence of bubble pairs taken from video footage. The initial size of each bubble was 2 mm diameter and the frequencies of the oscillations were determined by image analysis. From ref (18).

Almost 40 years later, Ata (17, 18) used a high-speed video to record, extremely precisely, the coalescence of equal-sized bubble pairs grown from thin steel capillary nozzles in solutions of surface-active particles and weak chemical surfactants. Initially, the solutions were introduced into the perspex container and two independent microsyringes with pump systems were used to generate air which was fed through two narrow capillaries to produce two identically sized bubbles. The bubbles were then gradually brought into contact using an electronic linear actuator. The coalescence time, which was defined as the time interval from the initial point of bubble contact to film rupture, was determined using a high-speed video camera. A schematic representation of the equipment used in the experiments is presented in Fig. 6.13.

Following rupture of the film, the bubbles were subjected to a series of rapid oscillations which were recorded (Fig. 6.14).

Using this technique, initial experiments were carried out with bubbles coated partially with hydrophobic particles which were detached from the surface during the coalescence process (17). Further experiments were carried out to compare the performance of a weak chemical frother (MIBC) with an inorganic electrolyte (NaCl) at a range of concentrations, and differences in bubble coalescence times were recorded and analyzed, together with data on the oscillation frequencies following the rupture event (18). The results were discussed with possible implications for the froth flotation process. In Fig. 6.15, a comparison is shown for MIBC and NaCl in which the coalescence time (seconds) versus concentrations plots are shown.

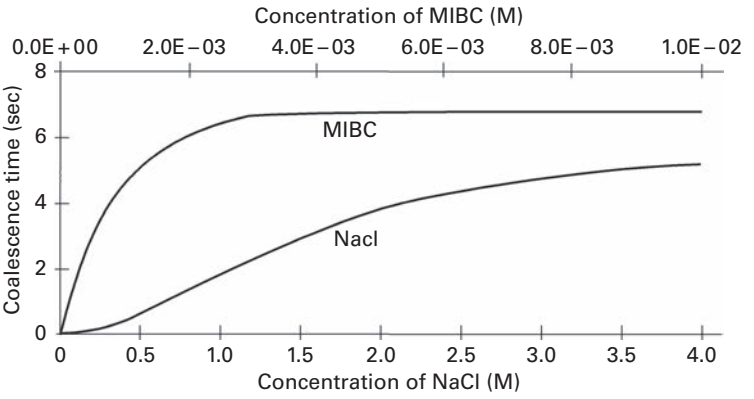

Fig. 6.15 Coalescence time as a function of concentration for MIBC and NaCl. From ref (18).

From these results, it was found that a much smaller amount of MIBC was needed to delay the coalescence process compared to the NaCl solution. Maximum coalescence time was reached at an MIBC concentration of 3×10^{-3} M, and beyond this concentration further addition of MIBC did not improve the stability of the bubble pairs any further. In the case of NaCl, increasing concentrations (from about 0.1 to 0.5 M) did not significantly delay the coalescence, but in the intermediate concentration range (0.5 to 3 M) a gradual increase in coalescence time was observed before slowly leveling off as the concentration approaches saturation. From this study it can be seen that MIBC is much more efficient at stabilizing bubbles than the NaCl, and it was also shown to be particularly effective at much lower concentrations (a few orders of magnitude). However, in plant flotation processes with particles present, a much lower concentration of MIBC was used ($\sim 10^{-4}$ M). In the flotation of hydrophobic particles in an aqueous NaCl solution as reported by Paulson and Pugh (19), small bubble size distributions have been reported and foams of transient stability were generated; it was suggested that the enhanced bubble stability in the froth zone was due to the attached particles.

The post-rupture bubble oscillation profiles obtained by Bournival and coworkers (18) for NaCl and MIBC were modeled as a linear, damped and harmonic oscillation process using a second-order differential equation which enabled the damping function of the oscillations to be calculated. In Fig. 6.16, the relationship between the damping constant and the concentration of both NaCl and MIBC is shown, and these plots indicate that more damping occurred with MIBC, possibly associated with the interfacial properties. Although the viscosity of NaCl solution increases with concentration, no pronounced damping was observed.

It was concluded that although NaCl was almost as effective as MIBC in preventing bubble coalescence, considerably greater concentrations are required. In 2014, additional experiments were carried out by Bournival and coworkers (20), and bubble coalescence and post-rupture oscillation results were obtained from several different types of low molecular weight nonionic surfactants such as 1-pentanol and 4-methyl

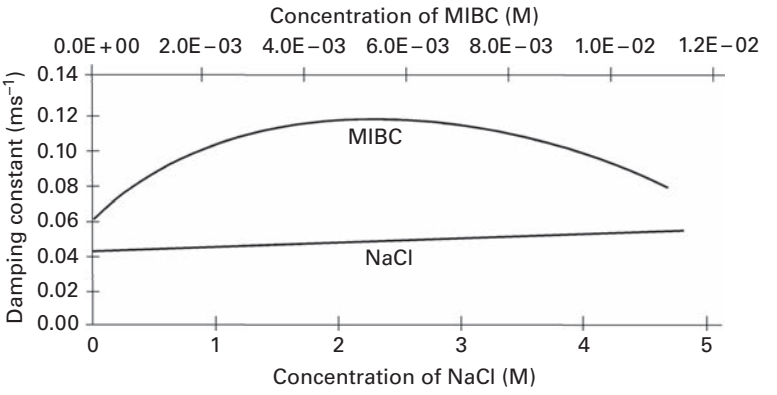

Fig. 6.16 Comparison of the damping constant at various concentrations of MIBC and NaCl. From ref (18).

(-2 pentanol). Analysis of these data revealed that the coalescence time increased with concentration of surfactant for all these nonionic systems, and a minimum amount of elasticity was required to achieve the increase in damping of the oscillations. However, it was suggested that the surface elasticity could not completely account for the damping and it was found necessary to take into consideration diffusion of surfactant to the bubble surface – which had a detrimental influence on the dynamic behavior of the bubble and reduced the damping.

6.5 Coalescence in aqueous solution of electrolytes

It has been well known for several decades that inorganic electrolytes have a positive effect on the generation and stability of bubbles, but this behavior was found by many researchers at first to be completely surprising, since it appears to be contradictory to the predictions of classical DLVO theory. In 1976, Melvile and Matijevic (21) generated bubble swarms by bubbling (sparging) an electrolyte solution and showed that the type and concentration of inorganic electrolyte greatly influenced the size and stability of the microbubbles. In Fig. 6.17 (a) and (b), the mean bubble diameter (determined by photographic size analysis) as a function of different electrolyte concentrations is shown. It was found that the bubble diameter decreased with increasing concentration toward a limiting value of about 100 μm. The nature of the ionic species had a pronounced influence on the bubble size, and for the Na^+, it was found that the divalent anion SO_4^{2-} was more efficient in reducing the size than monovalent Cl^- and NO_3^-. Also, for the NO_3^-, the divalent cations Ca^{2+} and Fe^{3+} were more effective than K^+.

In 1993, sparging experiments with aqueous solutions of inorganic electrolytes were carried out in a glass column by Craig and coworkers (8). From this study the "transitional concentration" which corresponded to the change from coalescence to stability with different electrolytes (as judged by a reduction in 50% in turbidity) was documented. The results were reported in terms of a particular combination of anions and cations

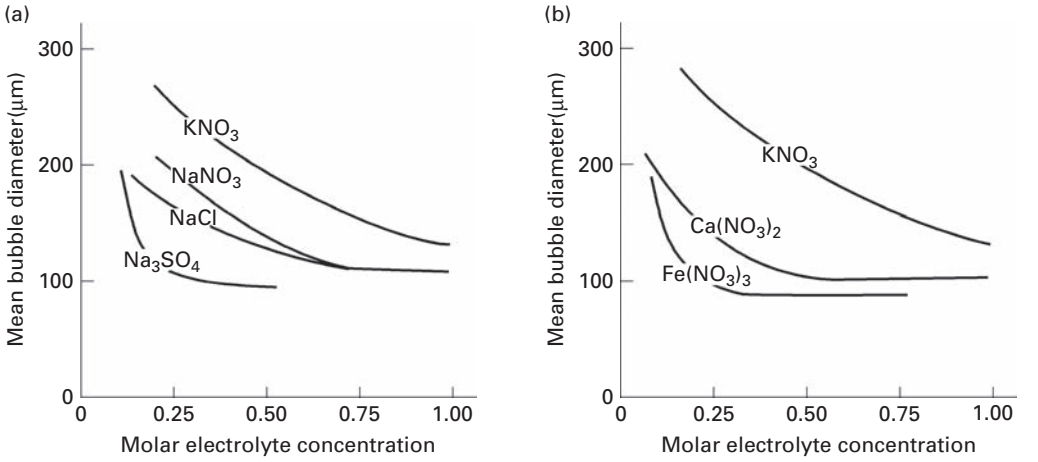

Fig. 6.17 Mean bubble diameter as a function of electrolyte concentration for bubbles produced by sparging gas through a sieve. Gas flow rate of 150 ml min^{-1}. From ref (21).

which could inhibit coalescence, and this led to a "combining rule" based on the nature of the cationic–anionic pairs which suggested that one could predict whether or not the electrolyte would inhibit coalescence. An explanation for the inability of some electrolytes to inhibit coalescence was not apparent, but these workers discarded the influence of surface tension gradients (which were relatively low) and suggested that the stabilization could be due to the resistance to thinning caused by a reduction in hydrophobic attraction forces. These workers incorrectly thought that the hydrophobic attraction between the bubble interfaces could be hindered by the specific adsorption of electrolyte, and it was only later that it was found that the hydrophobic attraction was most probably caused by the spontaneous formation of sub-micrometer gas-filled capillary bridges within the film. However, these new theories on hydrophobic attraction sparked a resurgence in research on the electrolyte effects on bubble coalescence.

In the experiments by Craig and coworkers (8), the maximum concentration of electrolyte used was about 0.5 M, but following this paper, Christenson and Yaminsky (7) found that the electrolytes that did not inhibit coalescence did so at higher concentration. These workers suggested that surface tension gradients (Gibbs-Marangoni) also played an important role in bubble coalescence in electrolytes. Weissenborn and Pugh (22, 23) measured the surface tension gradients ($d\,(\Delta\gamma)/dc$) using the dynamic bubble pressure method of a large range of electrolytes (36 in total) as a function of concentration up to 1 M and the values were significantly lower than for organic surfactants. The results for 1:1 (Fig. 6.18) and 2:1 and 3:1 (Fig. 6.19) electrolytes were discussed in terms of specific ion effects (the positive and negative adsorption of ions at the gas/liquid interface). It was found possible to correlate $d\,(\Delta\gamma)\,/dc$ with the degree of the hydration of the cation for electrolytes with bivalent ions ($MgCl_2$ and Na_2SO_4) that showed higher values of $d\,(\Delta\gamma)/dc$. Further correlations were obtained with the Jones–Dole viscosity coefficients and dissolved oxygen gradients. A calculation of

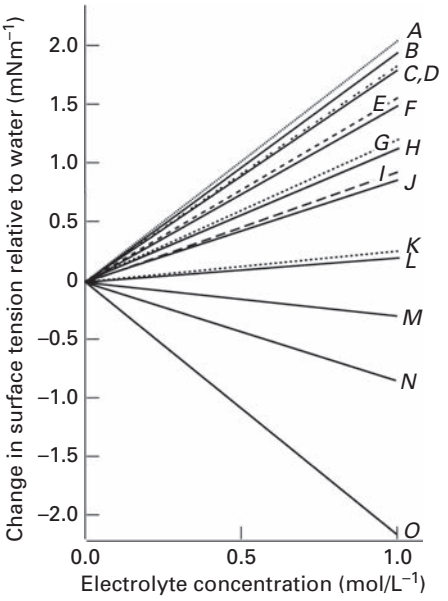

Fig. 6.18 Effect of electrolyte concentration on the change in surface tension of water for 1:1 electrolytes. A; NaCl, B; LiCl, C; KOH, D; KCl, NaBr, E; NaF, F; NH_4Cl, G; CsCl, H; NaI, I; NH_4NO_3, J; $NaClO_3$, $(CH_3)_4NCl$, K; $LiClO_4$, L; $NaClO_4$, M; HCl, N; HNO_3, O; $HClO_4$. Experiment carried out using the bubble pressure method with bubble interval 1.5 s. Error in data plus or minus 0.1 mN m^{-1}. From ref (22, 23).

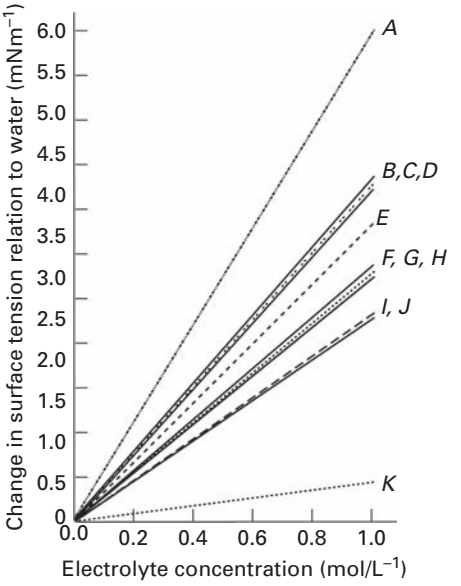

Fig. 6.19 Effect of electrolyte concentration on the change in surface tension of water for 2:1 and 3:1 electrolytes. A; $LaCl_3$, B; $Cr(NO_3)_3$, C; $MgCl_2$, D; $CaCl_2$, E; Li_2SO_4, F; $CaSO_4$, G; $Cr(NO_3)_3$, H; Na_2SO_4, I; $Ca(NO3)_2$, J;$MgSO_4$, K; H_2SO_4. Experimental carried out using the bubble pressure method with bubble interval 1.5 s. Error in data plus or minus 0.1 mN m^{-1}. From ref (22, 23).

the Gibbs surface deficiencies for selected electrolytes was reported, and discussions of $d(\Delta\gamma)/dc$ were extended to the mechanism of bubble coalescence. Although the Gibbs–Marangoni effect did not provide a complete explanation for the inhibition of coalescence for all the electrolytes, it was shown that it clearly played an important role, although it was suggested that dissolved gas gradients also needed to be taken into consideration.

Paulson and Pugh (19) in 1996 also reported that the flotation response of graphite was influenced by the type of electrolyte, and the highest flotation response occurred with the more strongly hydrated ions.

6.6 Influence of bubble approach velocity on bubble coalescence

Several early studies on bubble coalescence considered the influence of the bubble approach speed on the coalescence process. In 1967, Marrucci and Nicodemo (24) reported that the coalescence of bubbles generated through a porous plate in a column was influenced by the gas flow rate, which is related to the velocity. Kirkpatrick and Locket (11) in 1974 carried out bubble rise experiments in which the speed of bubble approach to a flat surface was varied by changing the release height. When the experiments were carried out in distilled water, it was found that coalescence occurred with the surface at approach speeds of less than 10 mm/s, while the bubbles rebounded from the interface at approach velocities greater than 100 mm/s. In 2002, Lehr and coworkers (25) measured the relative velocity of colliding bubbles in columns and observed that the final result of the collision (coalescence or bouncing) was dependent on the relative approach velocity and concluded that the velocity needed to be below a critical value for coalescence.

In 2011, Zawala and Malysa (26) studied the coalescence of bubbles in aqueous solutions of short-chain *n*-alcohols and showed that bubbles bounce from the interface if their approach speed produces a large area of deformation, and for coalescence to occur the area of deformation on approaching contact needed to be below a critical value. It was also shown that bubbles rebound from a surface at speeds in excess of about 100 mm/s. Chester and Hoffman (27) proposed a model and estimated that two bubbles should bounce apart without coalescence if their approach speed exceeds a critical value expressed by a velocity V_{ch}, which is defined by the equation

$$V_{ch} = (\gamma/2\rho\ R_b)^{1/2} \tag{6.9}$$

where R_b is the radii of two equal-sized bubbles and V_{ch} is essentially independent of electrolyte concentration. Klaseboer and coworkers (28) derived a value for the approach speed based on a numerical solution for the drainage of a thin film between two approaching spheres (bubbles) with immobile surfaces. They showed that as the bubbles flatten, dimpling occurs at a critical thickness, and the thickness of the barrier rim reaches about half of the flattering separation. They considered this thickness as the

minimum thickness (h_m) at which coalescence occurs, and this parameter was related to the Klaseboer approach velocity V_k by the equation

$$V_k = (\gamma/\eta)(h_m/0.2\ R_b)^2 \tag{6.10}$$

Much more revealing data on the relationship between approach speed and rupture were obtained in 2008 and 2009 by Horn and coworkers (29, 30, 31). These researchers modified a film pressure balance equipment so that it could operate at different approach speeds. Their results tended to support early models which related the surface tension gradients and interfacial elasticity to bubble coalescence in salt solutions. However, in addition, it was suggested that different mechanisms could also operate at low and high bubble approach speeds which act to delay bubble coalescence. From initial experiments (29) in freshly purified water at low approach speed (< 1 μm/s), it was shown that a flat fairly stable film was formed (100 nm thick) which was stabilized by the equilibrium disjoining pressure and that there was an electrostatic charge at the air/water interface of −57 mV caused by adsorbed atmospheric CO_2. The thin films were found to have moderate lifetimes (from 10 to 100 s) and withstood significant mechanical disturbances without breaking. In this case, there was no evidence of a hydrophobic force and no evidence of either hydrodynamic effects or dimpling caused by normal dynamic stresses which are commonly associated with drainage. Yaminsky and coworkers (30) also used DLVO theory to calculate the lowest concentration of univalent electrolyte required to stabilize the thin film, which was of the order of 10^{-4} M. In addition, it was found possible to derive a relationship between the critical Yaminsky approach speed (V_{y1}) and electrolyte concentration which was expressed by

$$V_{y1} = (4/3)^3(1/\gamma\eta)\ [\Delta\gamma_0 + c(d\gamma/dc)]^2 \tag{6.11}$$

where $\Delta\ \gamma_0$ is a small surface tension difference caused by variations in ionic adsorption created by one or two different mechanisms discussed in their paper. The best fit to their data was obtained with $\Delta\ \gamma_0 = 0.07$mN/m in pure water. At intermediate speeds (10^{-3} to 10^{-1} mm/s) transient foams were observed with lifetimes from 10 to 100 s, due to slow viscous drainage effects which delayed the coalescence, and it was proposed that electrostatic double layers no longer prevail.

A simple quantitative model was adopted from the Marrucci theory (4) based on a small surface tension gradient that provided sufficient surface elasticity to effectively immobilize the interface. However, at more rapid approach speeds, such immobilization cannot occur, and it was suggested that the film drains with a reduced hydrodynamic drag. From these studies, it was possible to derive an equation which described the spread of the tangential stress in a liquid film draining radially between two approaching bubbles. This was expressed in terms of the surface tension gradient and the bubble approach velocity ($V = -dh/dt$) as

$$V_{y2} \sim 16\ h/9\ \Delta\gamma\eta\ R_b \tag{6.12}$$

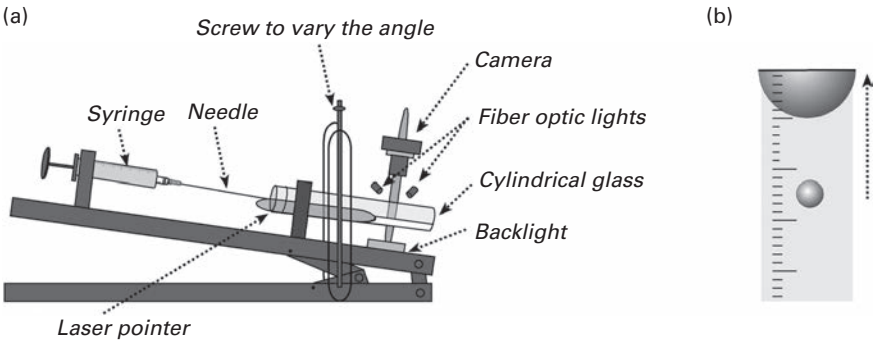

Fig. 6.20 (a) Experimental set-up for bubble–meniscus coalescence experiments at various approach speeds, (b) image of a small bubble (diameter about 1.6 mm) approaching the meniscus of the liquid at the upper end of the inclined glass chamber. Graduations on the cylinder and the bubble injection needle are visible. From ref (30).

Further experiments using an improved thin film apparatus, as shown in Fig. 6.20(a), enabled the interaction of two air bubbles approaching at different velocities (from 0.01 to 140 mm/s) to be more accurately monitored. The experimental set-up enabled small disjoining and viscous drag pressures and the flow patterns in the turbulent liquid films caused by Marangoni trace contaminants to be recorded. Air bubbles were released at the lower end of the graduated glass cylinder and slid up along the inside of the cylinder to approach the air/water meniscus (Fig. 6.20(b)). The velocity of approach was changed by changing the angle of inclination and measured by a laser technique. The complete process was monitored with a high-speed camera.

Experiments were carried out with both purified water and different concentrations of salt solutions. This study verified the earlier work and also presented a more detailed account of the mechanism for inhibiting coalescence at both high and low approach speeds. The time of arrival of the bubble at the interface was found to be followed by an induction time interval before rupture occurred which corresponded to the coalescence time. In some cases, at high speeds in salt solution, the bubbles bounced back and coalescence only occurred after several bounces. Throughout the study, transition speeds were recorded and the coalescence step was classified into separate regimes: stable (few minutes to a few hours), transient stability (stable for a few seconds) and instantaneous coalescence. These stability regimes were then related to both approach speed and the NaCl concentration.

These workers also reviewed published models and highlighted the most important parameters that influence the coalescence process (31). These were identified as viscous and inertial drainage, surface deformation, surface elasticity, mobility at the air/water interface and DLVO stability. The data were collected and collated in a single chart (Fig. 6.21) which presented the salt concentration and the bubble approach speed as the axes. The regions where the different mechanisms, where applicable, were mapped out. Boundaries between different coalescence regions, ranging from fairly concentrated to extremely dilute NaCl solutions, were identified. Although this chart highlights the different mechanisms involved in the coalescence process, it is restricted to both

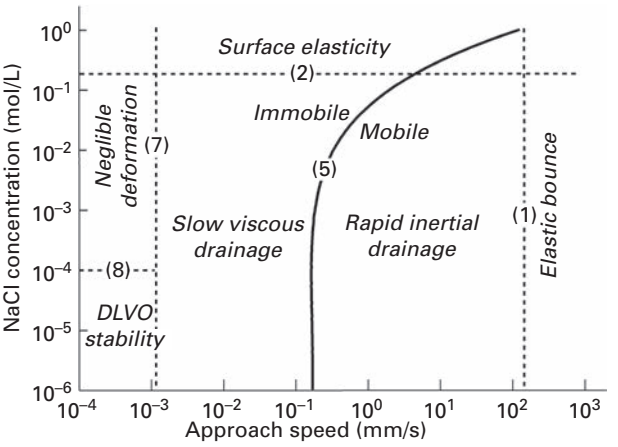

Fig. 6.21 Coalescence of bubbles in NaCl solution on a log-log scale to indicate where transitions between different types of mechanisms that occur at different velocities are indicated. The different regions were calculated by Horn (31), based on a 4 mm diameter bubble. From ref (31).

millimeter-sized bubbles and NaCl solution (at room temperatures). The influence of bubble size, different types of electrolyte, temperature, gas type, liquid viscosity or Reynolds number was not considered.

From the chart it can be seen that in both extremely pure water and dilute salt concentration the bubbles are stable at fairly low approach speeds (10^{-3} mm/s) due to electrostatic stabilization (DLVO theory), but at higher bubble approach speeds (just over 10^{-3} mm/s) electrostatic double layers no longer prevail, and it was suggested that hydrodynamics effect (slow viscous drainage) comes into play. In this region, the films in dilute salt solution are transiently stable, delaying the coalescence process by 10–100 s. These transient films collapse, usually after the contact area ceases to expand, and the films attain a state of hydrostatic equilibrium. By increasing the approach speed, an initial rapid expansion rate and an increase in contact area were observed, but the final lifetime of the film was reduced and dimples occurred. It was argued that a dramatic reduction in hydrodynamic resistance was caused by a transition from viscous-controlled drainage to rapid inertia-controlled drainage, which was associated with a change from immobile to mobile interface at increasing speeds of approach. Finally, at very high speeds both bubble deformation and flattening in the immobile regime occur which slowed down drainage and enabled the bubbles to rebound from the interface in both water and salt solutions. However, at high salt concentrations, surface elasticity is shown to be the important mechanism for stabilizing bubbles.

6.7 Influence of temperature on coalescence

There have been several early papers covering the effect of temperature on coalescence both in pure liquids and in weak surfactant solutions, but overall the results

are generally contradictive. In 1976, Sagert and Quinn (15) reported that temperature had little influence on coalescence of hydrogen sulfide (H_2S) bubbles in water measured on adjacent nozzles at three different temperatures. In 1983, Drogaris and Weiland (32) reported a decrease in coalescence time with rising temperature for bubble pairs formed at adjacent capillary tubes in aqueous solutions of *n*-alcohol and fatty acids. In 1993, Craig and coworkers (8) carried out experiments with bubble swarms stabilized in aqueous solutions of inorganic electrolytes in a column and observed a decrease in bubble coalescence with increase in temperature for aqueous solutions of NaCl and $MgSO_4$. In 1981, Quicker and Decker (33) reported data in non-aqueous systems and found the Sauter mean bubble diameter was independent of the operating temperature for N_2–xylene, N_2–decanlin and N_2–paraffin systems. Similar behavior was reported for N_2/water and N_2/cyclohexane

Ribeiro and coworkers (34) built an improved understanding of the temperature effects on coalescence from studies in pure liquids. Coalescence experiments were carried out in a cell in which bubbles were injected by a capillary located at the base of the cell. The bubble size was varied by adjusting the gas volume and introducing a vertical downward flow of liquid in the cell which met the ascending air bubbles. This resulted in the establishment of an equilibrium region where the bubbles could then be monitored. The motion of the bubbles and the recorded collisions between bubbles were observed by high-speed video camera. From the study, a quantitative criterion was developed to compute the critical velocity for bubble coalescence based on the outcome (coalescence or bouncing). In the study, two different liquids, water and ethanol, were used at four different temperatures. These experiments verified the existence of a so-called critical velocity, for coalescence and it was established that the rapid coalescence occurred at low approach velocities and increased with increase in approach velocities. It was also found that, contrary to previous data reported by Lehr (25), the critical velocity was a function of the physical properties of the liquid phase and the critical velocity increased with increase in temperature, which enhanced bubble coalescence. A linear dependence of the critical velocity upon the liquid temperature was verified for both fluids, as shown in Fig. 6.22, and the magnitude of the temperature effect was much greater for water than ethanol.

The coalescence process has been discussed in terms of the formation and deformation of the dimple in the liquid film between interacting bubbles, and it was proposed that the dimple played an important role in determining the critical velocity for bubble coalescence. Since the surface tension of ethanol is considerably lower than in water, bubble deformation and consequently dimple formation are easier in ethanol, but at higher temperatures there is a slight decrease in surface tension of both bulk fluids, enhancing dimple formation. However, the bulk viscosity of both liquids is reduced, thus enhancing the outward flow of liquid from the bulk to the liquid film. This leads to a lower hindrance in liquid flow for a given dimple shape, which suggests that to obtain the shape needed to eventually suppress coalescence, a higher degree of deformation or higher velocity of approach is

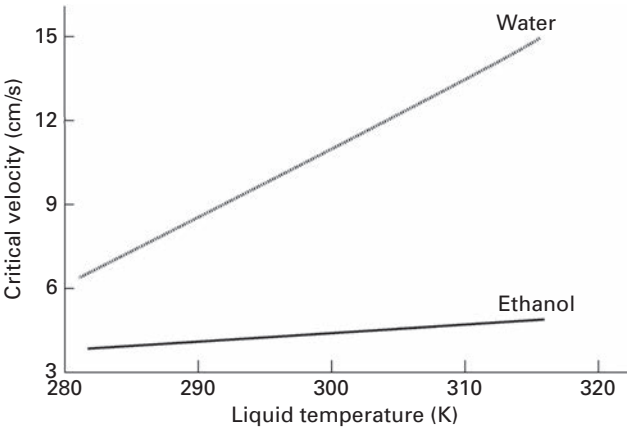

Fig. 6.22 Critical velocity for bubble coalescence as a function of liquid temperature for two different liquids. From ref (34).

required. In this study, models were also developed assuming immobility or partially immobile interfaces, and these could be used to predict the increase of bubble coalescence with the liquid temperature. It was concluded that in pure liquids thinning involves a viscous controlled mechanism.

References

(1) A. V. Nguyen and H. J. Schulze, *Colloid Science of Flotation*, Marcel Dekker, New York, 2003.
(2) P. C. Duineveld, Bouncing and Coalescence of Two Bubbles in Pure Water, *J. Fluid Mech.*, **31**, 151–60, 1995.
(3) S. I. Karashev, Dynamic and Expanding Foam Films under Additionally Applied Pressure, *Colloids Surf., A*, **372**, 151–154, 2010.
(4) G. Marrucci, A Theory of Coalescence, *Chem. Eng. Sci.*, **24**, 975–85, 1969.
(5) R. R. Lessard and S. A. Zieminski, Bubble Coalescence and Gas Transfer in Aqueous Electrolyte Solutions, *Ind. Eng. Chem. Fundam.*, **10**, 260–269, 1971.
(6b) M. J. Prince and H. W. Blanch, Bubble Coalescence and Break-up in Air Sparged Bubble Columns, *A.I.Ch.E. J.*, **36**, 1485–1499, 1990; (6a) M. J. Prince and M. W. Blanch, Transition Electrolyte Concentrations for Bubble Coalescence, *A.I.Ch.E. J.*, **36**, 1425–1429, 1990.
(7) H. K. Christenson and V. V. Yaminsky, Solute Effects on Bubble Coalescence, *J. Phys Chem.*, **99**, 10420–10420, 1995.
(8) V. S. J. Craig, B. W. Ninham and R. M Pashley, The Effect of Electrolytes on Bubble Coalescence in Water, *J. Phys. Chem.*, **97**, 10192–10197, 1993.
(9) R. D. Kirkpatrick and M. J. Locket, The Influence of Approach Speed on Bubble Coalescence, *Chem. Eng. Sci.*, **29** (12), 2363–2373, 1974.
(10) G. D. Burnett, J. J. Chae, W. Y. Tam, R. M. C. De Almeida and M. Tabor, Structure and Dynamics of Breaking Foams, *Phys. Rev., E*, **51** (6), 5788, 1995.

(11) H. Ritacco, F. Kiefer and D. Angevin, Lifetime of Bubble Rafts Cooperativity and Avalanches, *Phys. Rev. Lett.*, **98** (24), 2007.
(12) W. Kracht and J. A. Finch, Using Sound to Study Bubble Coalescence, *J. Colloid Interface Sci.*, **332**, 237–245, 2009.
(13) G. J. Jameson and V. Parekh, *Effect of n-Alcohols on the Rate of Coalescence of Bubbles, Proceedings of the Interfacial Phenomena in Fine Particle Technology*, 6th UBC Mc Gill-UA International Symposium, Montreal, Quebec, Canada, pp. 443–459, 2006.
(14) O. Bartsch, Foaming Power and Surface Tension, *Kolloid Z.*, **38**, 177–179, 1920.
(15) N. H. Sagert, M. J. Quinn, S. C. Cripps and E. I. J. Rosinger, Bubble Coalescence in Aqueous Solutions of n-Alcohols In *Foams*, Ed. R. J. Akers, Academic Press, New York, pp. 133–146, 1976.
(16) A. Sharma and E. Ruckenstein, Critical Thickness and Life-time of Foams and Emulsions; Role of Surface Wave-Inducing Thinning, *J. Colloid Interface Sci.*, **119**, 14, 1987.
(17) S. Ata, Coalescence of Bubbles Coated with Particles, *Langmuir*, **24** (10), 6085–6091, 2008.
(18) G. Bournival, R. J. Pugh and S. Ata, Examination of NaCl and MIBC as Bubble Coalescence Inhibitors in relation to Froth Flotation, *Miner. Eng.*, **25** (1), 47–53, 2012.
(19) O. Paulson and R. J. Pugh, Flotation of Inherently Hydrophobic Particles in Aqueous Solutions of Inorganic Electrolytes, *Langmuir*, **12**, 4808–4813, 1996.
(20) G. Bournival, S. Ata, S. I. Karakashev and G. J. Jameson, An Investigation of Bubble Coalescence and Post-rupture Oscillations in Nonionic Surfactants Solution Using High Speed Cinematography, *J. Colloid Interface Sci.*, **414**, 50–58, 2014.
(21) J. B. Melville and E. Matijevic, *Microbubbles; Generation and Interactions with Colloidal Particles in Foams*, Ed. R. J. Akers, Academic Press, London, pp. 217–236, 1976.
(22) P. K. Weissenborn and R. J. Pugh, Surface Tension and Bubble Coalescence Phenomena of Aqueous Solutions of Electrolytes, *Langmuir*, **11**, 1422–1426, 1995.
(23) P. K. Weissenborn and R. J. Pugh, Surface Tension of Aqueous Solutions of Electrolytes, Relationship with ion Radius, Oxygen Solubility and Bubble Coalescence, *J. Colloid Interface Sci.*, **184**, 550–563, 1996.
(24) G. Marrucci and L. Nicodemo, Coalescence of Gas Bubbles in Aqueous Solutions of Inorganic Electrolytes, *Chem. Eng. Sci.*, **22**, 1257–1265, 1967.
(25) F. Lehr, M. Millies and D. Mewes, Bubble-Size Distribution and Flow Fields in Bubble Columns, *A.I.Ch.E. J.*, **48**, 2426–2443, 2002.
(26) J. Zawala and K. Malysa, Influence of Impact Velocity and Size of the Film Formed on Bubble Coalescence Time at Water Surface, *Langmuir*, **27**, 2250–2257, 2011.
(27) A. K. Chester and G. Hoffman, Bubble Coalescence in Pure Liquids, *Appl. Sci. Res.*, **38**, 353–361, 1982.
(28) E. Klaseboer, J. Ph. Chevaillier, C. Gourdon and O. Masbernat, Colliding Drops at Constant Approach Velocity: Experiments and Modelling, *J. Colloid Interface Sci.*, **229**, 274–285, 2000.

(29) V. V. Yaminsky, S. Ohnishi, E. A. Volgler and R. G. Horn, Stability of Aqueous Films between Bubbles. Part 1 The Effect of Speed on Bubble Coalescence in Purified Water and Simple Electrolyte Solutions, *Langmuir*, **26** (11), 8061–8074, 2010.
(30) L. A. De Castillo, S. Ohnishi and R. H. Horn, Inhibition of Bubble Coalescence: Effects of Salt Concentration and Speed of Approach, *J. Colloid Interface Sci.*, **356**, 316–324, 2011.
(31) R. H. Horn, L. A. De Castillo and S. Ohnishi, Coalescence Map for Bubbles in Surfactant-Free Aqueous Electrolyte Solution, *Adv. Colloid Interface Sci.*, **168**, 85–92, 2011.
(32) G. Drogaris and P. Weiland, Studies of Coalescence of Bubble Pairs, *Chem. Eng. Commun.*, **23**, 11–26, 1983.
(33) G. Quicker and W. D. Decker, Gas Hold-Up and Interfacial Area in Aerated Hydrocarbons, *Chemie Ing. Tech.*, **53**, 474–475, 1981.
(34) C. P. Ribeiro Jr and D. Mewes, On the Effect of Liquid Temperature upon Bubble Coalescence, *Chem. Eng. Sci.*, **61**, 5704–5704, 2006.